Peer-reviewed version available at *Molecules* **2018**, *24*, 79; doi:10.3390/molecules24010079

Article

Quantification of σ–holes and their use as a descriptor for the theoretical calculation of p*K*a values for carboxylic acids

Guillermo Caballero-García [1], Gustavo Mondragón-Solórzano [1], Raúl Torres-Cadena [1], Marco Díaz-García [1], Jacinto Sandoval-Lira [1], Joaquín Barroso-Flores [1,*]

[1] Centro Conjunto de Investigación en Química Sustentable UAEM – UNAM, Carretera Toluca–Atlacomulco km 14.5, Unidad San Cayetano, Personal de la UNAM, Toluca 50200, Estado de México, Mexico; jbarroso@unam.mx

* Correspondence: jbarroso@unam.mx; Tel.: +52-722-2766610 Ext 7754

Abstract: Theoretical approaches to calculate p*K*a values for Brønsted acids is a challenging task that, most of the time, involves sophisticated and time-consuming methods. Therefore, heuristic approaches are efficient and appealing methodologies to approximate these values. Herein, by considering the electrostatic potential on acidic hydrogen atoms in a similar fashion that a σ–hole is defined, we calculated the maximum surface potential, $V_{S,max}$, and used it as a descriptor to correlate it with experimental acidity constants. These values were calculated using the CPCM implicit solvent model (*water*) with six different methods: five density functionals and the Møller–Plesset second order perturbation theory. Six different basis sets were combined with each method in order to benchmark a total of thirty-six levels of theory. Overall, 1080 calculations were performed and found to correlate with experimental data. The ωB97X-D/6-31+G(*d*,*p*) level of theory stands as the best one for consistently reproduce the reported p*K*a values.

Keywords: p*K*a; Hydrogen Bond; σ–hole.

1. Introduction

The term '*tetrel bond*' was first used by Frontera in 2013 to designate the directional, intermolecular and non-covalent interactions of electrostatic nature involving elements in group 14. These atoms behave as electrophiles through their interaction with either *n* or π electrons from Lewis bases [1,2]. Such interactions are similar to those observed for elements in groups 15 and 16, which are termed pnictogen and chalcogen bonds, respectively. The formation of these non-covalent interactions stems from a similar origin as halogen bonds, *via* the presence of σ–holes [3–5], a localized region of positive electrostatic potential on the surface of the group 17 atom and opposite to the internuclear axis of a covalent σ bond, hence σ–holes. Therefore, tetrel bonds belong to a broader kind of directional non-covalent electrostatic interactions like halogen [6–8], chalcogen [9,10], and pnicogen bonds [11]. A stretch of this label has been applied to hydrogen bonding, despite the absence of *p* electrons on hydrogen atoms and the high polarizability of their bonds [12,13].

Tetrel bonds are stabilizing interactions in nature [14,15] that are able to form cooperative networks [9,16–20], a feature that is used as a powerful tool for the design of crystal structures [21–23]. The stabilization arising from these interactions ranges from 1 kcal/mol to 50 kcal/mol [24]. The strength of the interaction increases as the tetrel atom increases its atomic number; the electronegativity of the atom bonded opposite to the tetrel bond; and the number of electron withdrawing groups bonded to the tetrel atom. Therefore, the formation and strength of a tetrel

Peer-reviewed version available at *Molecules* **2018**, *24*, 79; doi:10.3390/molecules24010079

bond depend closely on the polarization of the electron density surrounding the tetrel atom. These factors have been extensively investigated by Scheiner, who has further divided them into electronic [24,25] and steric [26] contributions.

Experimentally, tetrel bonds have been observed by means of ^{1}H, ^{13}C, and ^{207}Pb NMR techniques [27–29], as well as through X-ray diffraction methods from which their effects in the formation of crystal structures is obtained by direct measurements [21,23,30], including systems where tetrel–tetrel bonds are formed [31]. However, their interesting electronic structure is the feature that has attracted most of the research. Several computational studies on their nature have been published so far, from their strict quantum treatment [32] to their charge transfer dynamics in the attoseconds regime [33] and the tunneling bond-breaking processes promoted by σ-holes [34]. Studies regarding the specific features for each kind of derivatives of the tetrel atoms are reported. These include silicon oxide based compounds such as silanol, siloxane and others [35–37]; tin and lead compounds [38]; unsaturated hydrocarbons [39,40], carbenes[41], anionic species [42–44]; and even single–electron tetrel bonds involving the $\cdot CH_3$ radical species [45]. Non–tetrel atoms such as halogens [44,46], or beryllium bonded compounds which are able to induce the formation of σ–holes [47,48] have also been studied.

Unsaturated carbon species can also form tetrel–bonds involving their π electron density with various electron rich donors such as CO, CS [49] and OCS with nitrogen bases [50–52], σ–π bonded complexes [4,53], π–σ-hole [54] bonded complexes and cation–π interactions [55], and π electrons bearing carbon compounds with potential applications for CO_2 capture [56–58].

Thus, the importance of the study of non–covalent interactions has large implications for crystal engineering [59], biochemistry and the understanding of chemical reactivity [60–62]. In our research group we have reported the chemical reduction of a trichloromethyl group into a methyl group *via* the attack of σ–holes on chlorine atoms by thiophenolate anions, a reaction mechanism which is extensible to other trichloromethyl compounds [63].

The hydrogen bond has become a paradigm among the toolbox of chemical concepts [64]. A strong, directional, non-covalent interaction that is responsible for a massive number of chemical phenomena [65–67]. The accurate prediction of p*K*a values for carboxylic acids by means of computational methods covers a wide range of potential applications from chemical design to drug development [68–70]. However, calculating the equilibrium constant for the deprotonation of a Brønsted acid implies the use of sophisticated and computationally intensive methods, such as G3MP2, to calculate solvation free energies for all the species involved in the associated thermodynamic cycle [71]. It is commonly regarded that the dissociation process is mainly controlled by electrostatic interactions, given the partial positive charge on the acid hydrogen. Since this interaction is not isotropic some parallel between hydrogen and σ–hole bonded systems arise. The formation of these directional interactions implies the presence of an electrostatic potential maximum located on the opposite side of the O–H σ–bond, which can be quantified by the maximum surface electrostatic potential, $V_{S,max}$. By postulating herein that the first stages of the deprotonation process of any given carboxylic acid occur through an interaction akin a tetrel or halogen bond between the acid and a water molecule, R-COOH···OH_2, we can use the $V_{S,max}$ value as an efficient descriptor that strongly correlates with the measured p*K*a value of a carboxylic acid. Previously, the nucleophilicities and electrophilicities of Lewis acids and bases, respectively, have been derived from interpolation of their mutual dissociation energies [72].

2. Results

Thirty (30) different carboxylic acids with reported p*K*a values were selected from Lange's Handbook of Chemistry [73], optimized and the surface electrostatic potential calculated (see methods section for full details). The structure of the acids are shown in Figure 1. The levels of theory used were obtained from the combination of the following functionals, ωB97X-D (**A**), B3LYP (**B**), LC-ωPBE (**C**), M06-2X (**D**) and PBE0 (**E**), as well as the Møller-Plesset second-order perturbation

Preprints (www.preprints.org) | NOT PEER-REVIEWED | Posted: 19 October 2018 doi:10.20944/preprints201810.0434.v1

Peer-reviewed version available at *Molecules* **2018**, *24*, 79; doi:10.3390/molecules24010079

theory, MP2 (**F**) and the following basis sets, 6-31+G(*d*,*p*) (**1**), 6-311++G(*d*,*p*) (**2**), cc-pVDZ (**3**), cc-pVTZ (**4**), aug-cc-pVTZ (**5**) and Def2-TZVP (**6**).

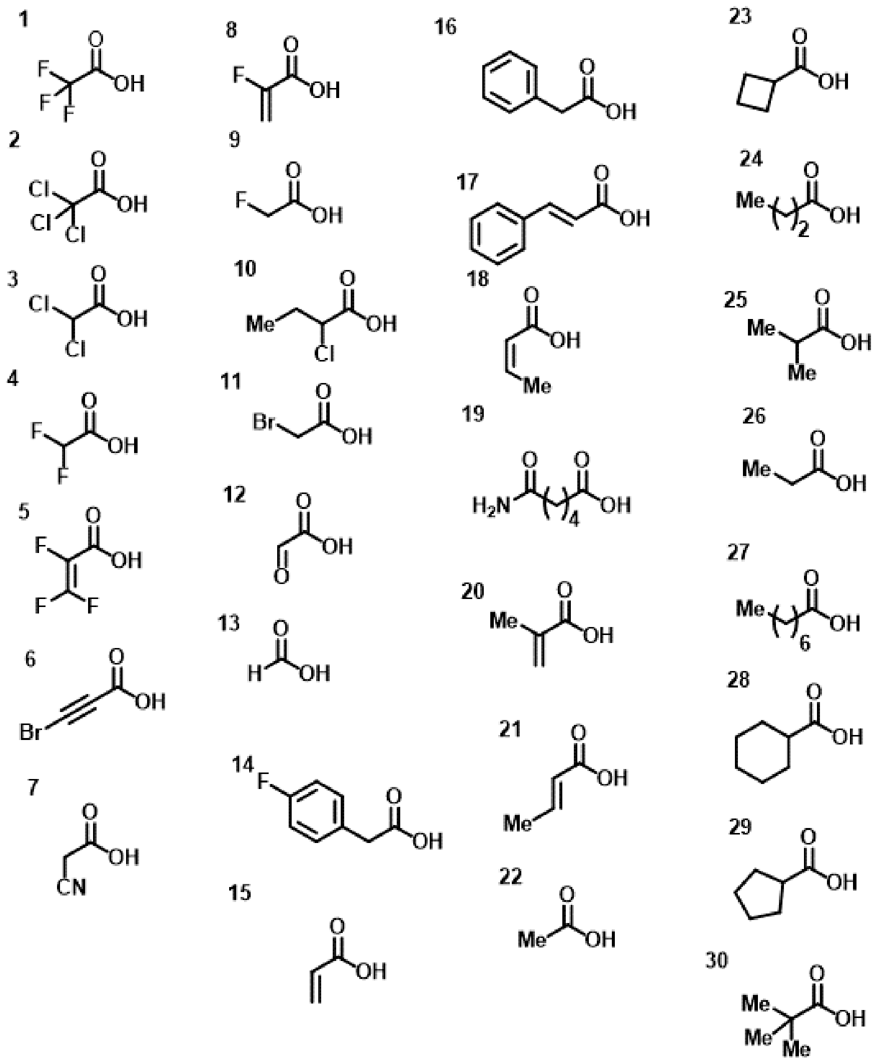

Figure 1. Thirty carboxylic acids comprising the chemical space under study.

In total, thirty-six levels of theory were used to calculate the electronic structure of the thirty carboxylic acids which comprise the chemical space under study for a total of 1,080 different wave functions upon which the maximum surface potential, $V_{S,max}$, was calculated and plotted against the experimental pKa_{exp} value. Simple linear regressions were performed to obtain the best fittings. The $V_{S,max}$ on each acidic hydrogen atom was used for the correlations, as an example, Figure 2 depicts the location of $V_{S,max}$ on the acid hydrogen atom for compound 14. This value is calculated on the isodensity surface $\varrho = 0.001$ a.u. and is used as a descriptor for the magnitude of a σ–hole equivalent on hydrogen.

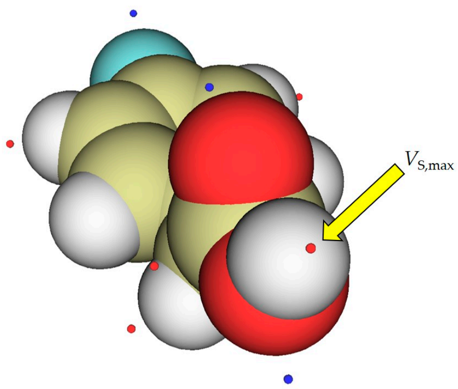

Figure 2. Maximum surface electrostatic potential, $V_{S,max}$, over the acidic hydrogen atom shown for compound 14 taking an isodensity value of 0.001 a.u. (isosurface not shown)

All correlation coefficients, slopes, and intercepts for all thirty-six levels of theory are collected in Table 1.

Table 1. Linear regression parameters obtained for the p*K*a vs. $V_{S,max}$ plots. Intercept units in kcal/mol

	slope	**Intercept**	R^2		**slope**	**Intercept**	R^2
A1	-0.1890	15.6915	0.9241	**D1**	-0.1935	15.9819	0.9310
A2	-0.1901	15.3454	0.9227	**D2**	-0.1893	15.1661	0.9315
A3	-0.2072	15.5189	0.9123	**D3**	-0.2133	15.7926	0.9002
A4	-0.2021	15.8188	0.9174	**D4**	-0.2007	15.7719	0.9225
A5	-0.1982	15.8367	0.9161	**D5**	-0.1765	14.5112	0.8796
A6	-0.2045	15.8616	0.9168	**D6**	-0.2033	15.6156	0.9200
B1	-0.1830	14.7367	0.8996	**E1**	-0.1867	15.3189	0.9084
B2	-0.1833	14.3499	0.8993	**E2**	-0.1860	14.8108	0.8973
B3	-0.2077	14.8807	0.8952	**E3**	-0.2035	15.1196	0.8955
B4	-0.1983	14.9381	0.8999	**E4**	-0.2007	15.4529	0.9016
B5	-0.1895	14.6298	0.8886	**E5**	-0.1937	15.2129	0.8963
B6	-0.20107	14.8703	0.8223	**E6**	-0.2017	15.3350	0.8954
C1	-0.1834	15.2811	0.8972	**F1**	-0.1937	15.5261	0.9046
C2	-0.1808	14.8234	0.9051	**F2**	-0.2033	15.4111	0.9041
C3	-0.2136	15.8429	0.9037	**F3**	-0.2183	15.7690	0.9158
C4	-0.1839	14.8594	0.8935	**F4**	-0.2099	15.7708	0.8957
C5	-0.2005	15.9657	0.9187	**F5**	-0.1999	15.4754	0.9005
C6	-0.2078	15.9734	0.9171	**F6**	-0.2085	15.5996	0.8927

The obtained linear model is shown in Figure 3 for method (**A**) only, the plots with the rest of the methods (**B**) – (**F**) are presented in the Supporting Information section (Figures S 1 to S 12).

Preprints (www.preprints.org) | NOT PEER-REVIEWED | Posted: 19 October 2018 doi:10.20944/preprints201810.0434.v1

Peer-reviewed version available at *Molecules* **2018**, *24*, 79; doi:10.3390/molecules24010079

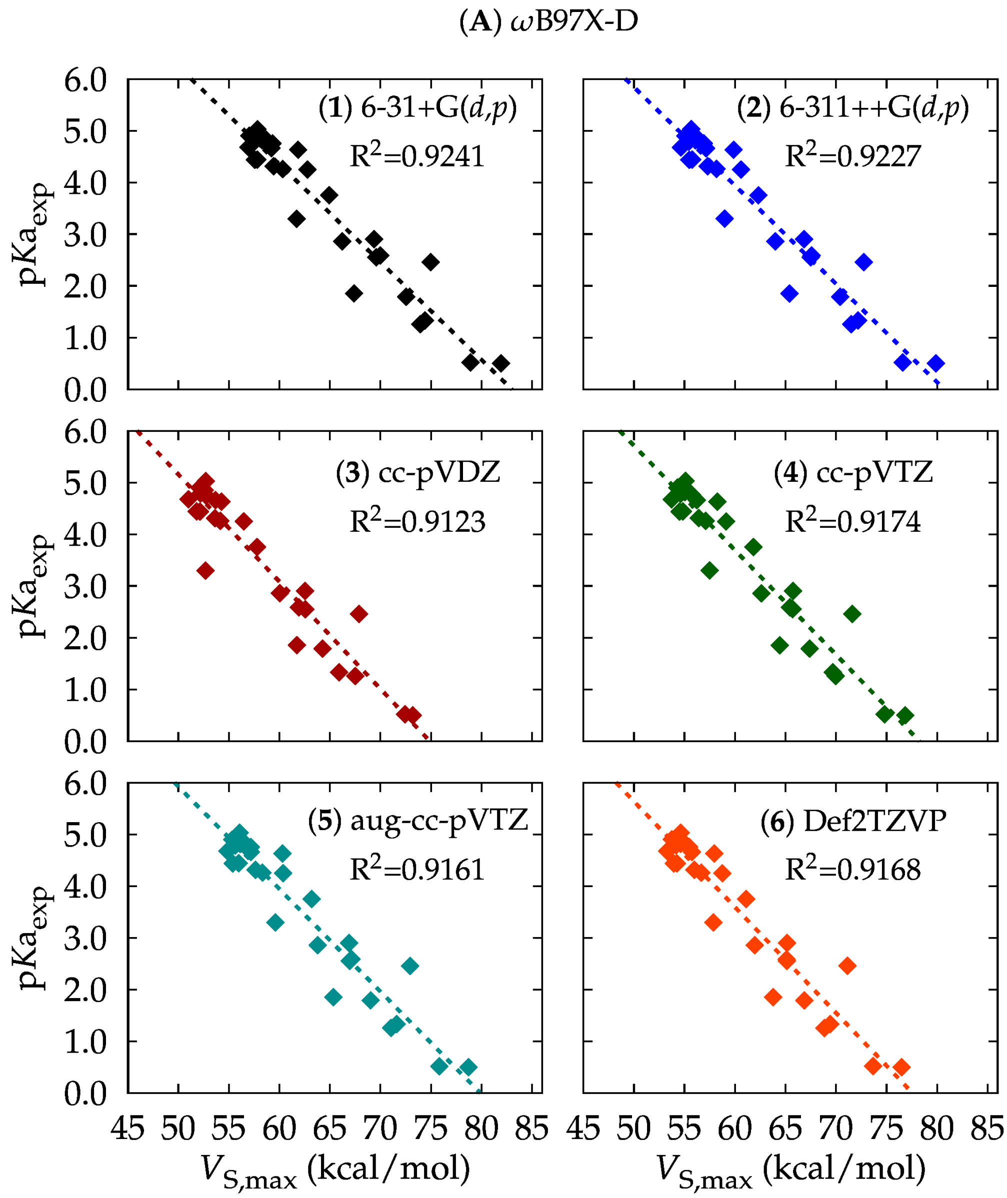

Figure 3. Linear correlations between pKa_{exp} against $V_{S,max}$ for DFT method (**A**) with the six basis sets (**1**) through (**6**).

To further analyze the obtained models, a comparison between experimental and calculated p*K*a values is made by calculating Δp*K*a = pKa_{exp} – pKa_{calc}. Figure 4 shows these plots for results obtained with the functional (**A**), the corresponding Δp*K*a plots for the other levels of theory are collected in the Supporting Information section (Figures S 1 – S 12).

Preprints (www.preprints.org) | NOT PEER-REVIEWED | Posted: 19 October 2018 doi:10.20944/preprints201810.0434.v1

Peer-reviewed version available at *Molecules* **2018**, *24*, 79; doi:10.3390/molecules24010079

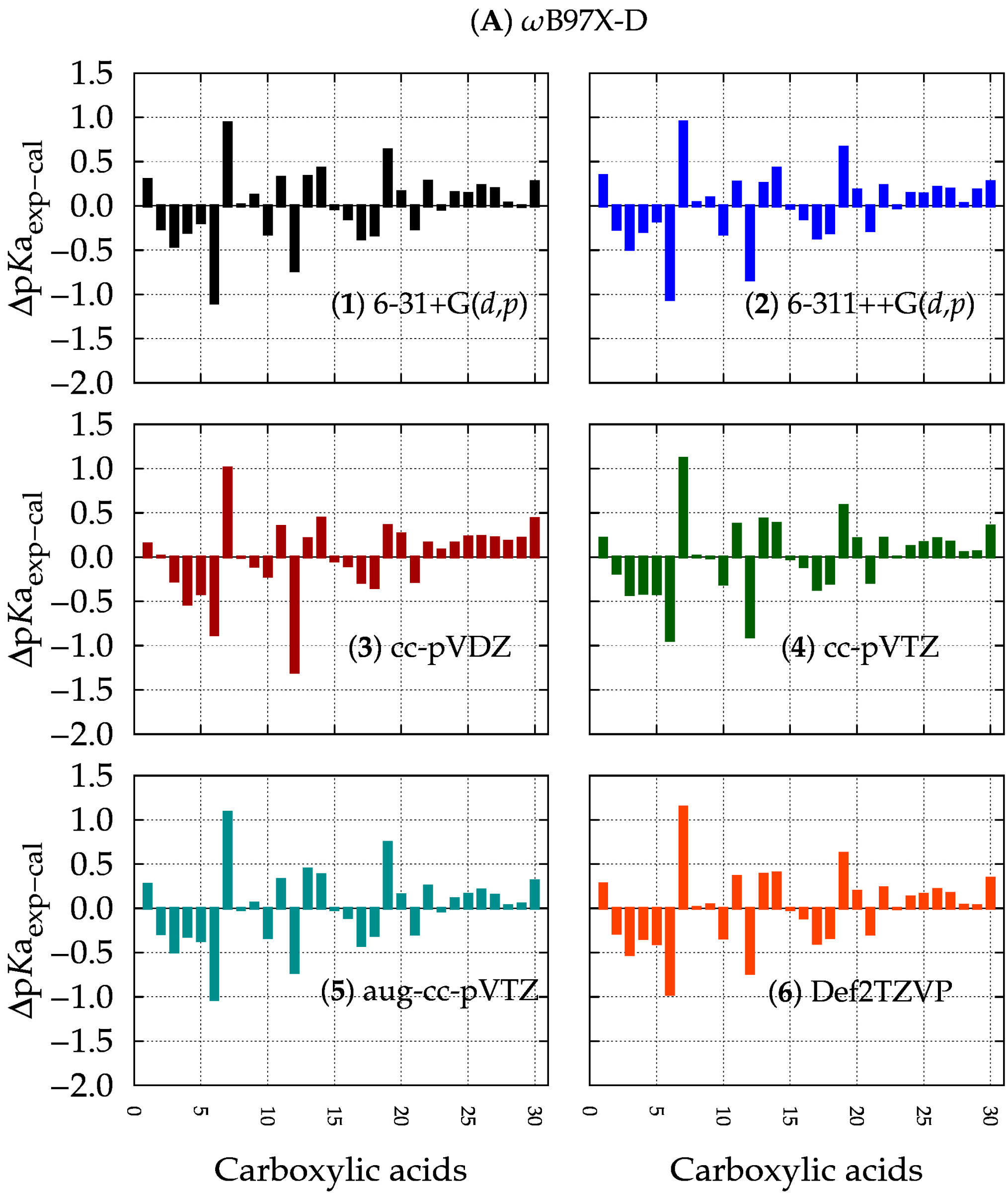

Figure 4. Δp*K*a = pKa_{exp} - pKa_{calc} for DFT method (**A**) with the six basis sets (**1**) through (**6**).

3. Discussion

3.1. Computational method: DFT or ab initio?

From all the tested levels of theory, the highest R^2 correlation coefficients (Table 1) between $V_{S,max}$ and pKa_{exp} values are obtained consistently with the ωB97X-D functional (**A**), whereas the lowest are obtained with the B3LYP functional (**B**). The latter method, albeit being one of the most popular ones to model organic molecules, could inadequately be describing the surface potential due to the lack of dispersion effects in the functional, which is not the case for ωB97X-D that includes implicit dispersion. A similar performance to that of B3LYP was observed for the PBE0 functional (**E**), and just slightly improved for LC-ωPBE (**C**). The latter functional was though to yield much better results due to the long range correlation term, however that was not the case.

The M06-2X functional (**D**) also shows to be properly describing the surface electrostatic potentials, as shown in the high correlation coefficients. This is plausibly because of the dispersion terms included in its formulation, which also applies for the ωB97X-D functional.

Although the M06-2X functional is widely used and regarded as probably the best functional to model organic reactions, yields a larger discrepancy in the Δp*K*a plots than those obtained with

Preprints (www.preprints.org) | NOT PEER-REVIEWED | Posted: 19 October 2018 doi:10.20944/preprints201810.0434.v1

Peer-reviewed version available at *Molecules* **2018**, *24*, 79; doi:10.3390/molecules24010079

ωB97X-D (Figures 4 and S 7). In sharp contrast with all the other tested functionals (**A**, **B**, **C** and **E**), the Minnesota functional has the largest values of Δp*K*a (Figure S 8), which indicates that may not be an adequate functional to estimate acidity constants using linear regressions.

As a benchmark comparison standard, the Møller-Plesset second-order perturbation theory, MP2 (**F**), was included in the study, not only to assess its accuracy, but to compare DFT and at least one wave function method as well. Despite of performing similarly to ωB97X-D yielding low error bars (Δp*K*a, Figure S 12), the correlation coefficients for the MP2 levels of theory were lower than those for ωB97X-D. This shows that, for the case of modeling surface electrostatic potentials, a computationally expensive method may not always be preferred, as very similar or even better results can be obtained with a less demanding approach in just a fraction of time.

Amongst the set of models obtained for (**A**), the **A1** level of theory has the highest correlation (R^2 = 0.9241) corresponding to the ωB97X-D/6-31+G(*d*,*p*).

3.2. Basis set: Is larger better?

Most of the reported benchmarks to model organic molecules deal with the DFT functional. However, little attention is payed to the basis set, or more precisely, to the proper functional/basis set combination. It is quite a common paradigm among computational chemists that the larger the basis set the better; therefore, using a CBS method as a benchmark standard, but how much is enough.

Four out of the six methods yielded the strongest $V_{S,max}$-p*K*a correlations when using the relatively medium size 6-31+G(*d*,*p*) basis set. This was not the case for the LC-ωPBE functional, which required the largest basis set (**5**) under study for a good correlation coefficient. Surprisingly, the M06-2X functional presented the largest Δp*K*a deviations when combined with the largest basis set aug-cc-pVTZ (Figure S 8).

In the case of the MP2 calculations (Figure S 11), increasing the so-called quality of the basis set may not be beneficial in all cases. When comparing the split-valence Pople's basis sets, practically the same correlation was found with the double-ζ set and the corresponding triple-ζ quality one, 0.9046 *versus* 0.9041, respectively. On the other hand, the Dunning-Huzinaga basis showed a deemed correlation when increasing the set size from cc-pVDZ to cc-pVTZ, 0.9158 and 0.8957, respectively. However, Δp*K*a deviations are practically consistent among the MP2 levels of theory.

In terms of the difference between experimental and correlated p*K*a values the **A1** level of theory yields the smallest Δp*K*a deviations with most of the differences kept under 0.5 p*K*a units, showing that, for this case, the larger the basis set size may not always be the better.

3.3. Limitations: A final remark

From the thirty-six levels of theory tested in this study, four compounds presented the largest Δp*K*a deviations: 6, 7, 12 and 19. This possibly be due to strong delocalization effects from nearby π bonds to the $\sigma^*_{O\text{-}H}$ orbital in the acidic hydrogen atom or intramolecular hydrogen bonding with Lewis basic motifs (Figure 5). For such kind of compounds, further improvements are required in the methodology for our linear models.

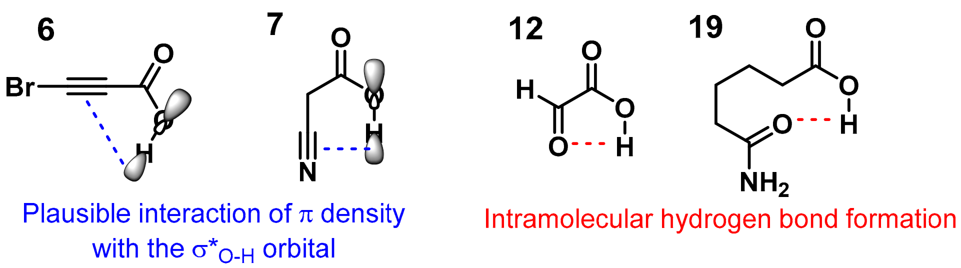

Figure 5. Electronic effects to be considered in further improvements of the method.

Peer-reviewed version available at *Molecules* **2018**, *24*, 79; doi:10.3390/molecules24010079

So far, the applicability domain of these regression is limited by the p*K*a data used to construct the models (0.5 < p*K*a < 5.0), caution must be taken when using the linear models presented herein for molecules outside this range.

4. Materials and Methods

Geometry optimizations and wave function printouts for the 30 carboxylic acids were performed using the Gaussian 09 rev. E01 suite of programs [74] at each of the different levels of theory (see text). All calculations included the CPCM implicit solvation model (*water*). Frequency analyses were done at the end of each geometry optimization at the same level of theory in order to verify that the found geometries corresponded to energy minima. Ultrafine integration grid was used in all the calculations.

The maximum surface potential calculations were performed on the wave function files with the MultiWFN program, version 3.3.8 [75] using an isodensity value of 0.001 a.u. All the computed values are collected in the Supporting Information (Tables S 1 to S 6).

5. Conclusions

With our calculations, $V_{S,max}$ has proven not only to be a suitable descriptor of the magnitude of a σ–hole, but a proper quantity that correlates with the p*K*a value of carboxylic acids as well. By means of DFT calculations with the use of a simple implicit solvent model (CPCM), the value of $V_{S,max}$ can be calculated and the equations obtained herein can be used to estimate p*K*a values without the need for a full thermodynamic cycle calculation, thus, avoiding long computations of solvation free energies and other costly quantities.

The ωB97X-D/6-31+G(*d*,*p*) level of theory (**A1**) yielded the lowest Δp*K*a values, standing as the best choice for estimating the p*K*a of any given acid through the calculation of $V_{S,max}$. Hence, we highly recommend this level of theory for geometry optimization and wave function file print. Care must be taken, as the p*K*a value sought after should be between 0.5 and 5.0 pH units.

Further testing is needed for these regression models to become universal. Inclusion of intramolecular hydrogen bonding as well as highly delocalizing features within the chemical space are key features to be considered in future improvements of the model. Our proposed descriptor is also dependent of the isodensity value for the definition of the surface upon which it is calculated, and it is highly recommended to keep the value suggested by Bader et al. [76] of ϱ = 0.001 a.u.

Supplementary Materials: The following are available online, Table S1-S6: Calculated V S,max values for carboxylic H atoms to the different levels of theory studied, Table S7: Reported pKa values for carboxylic acids studied. Figure S1-S5: Correlation of pKa exp vs VS,max. Figure S6-S10: Difference between the experimental and calculated pKa values (ΔpKa exp-cal).

Author Contributions: conceptualization, J.B-F. and G.C-G.; methodology, J.B-F.; G.C-G. and J.S-L.; validation, J.B-F. and J.S-L.; formal analysis, J.B-F.; G.C-G.; G.M-S and J.S-L.; data curation, G.C-G.; G.M-S.; R.T-C.; and M.D-G.; writing—original draft preparation, G.C-G and G.M-S.; writing—review and editing, J.B-F.; G.C-G. and J.S-L.; visualization, G.C-G., J.S-L and G.M-S.; supervision, J.B-F.; project administration, J.B-F.

Funding: This research received no external funding.

Acknowledgments: We thank DGTIC – UNAM for granting us access to their supercomputing facilities known as '*Miztli*'. We also thank Ms. Citlalit Martínez for keeping our local computational facilities running properly. JSL thanks DGAPA – UNAM for the postdoctoral scholarship.

Conflicts of Interest: The authors declare no conflict of interest.

References

1. Legon, A. C. Tetrel, pnictogen and chalcogen bonds identified in the gas phase before they had names: A systematic look at non-covalent interactions. *Phys. Chem. Chem. Phys.* **2017**, *19*, 14884–14896, doi:10.1039/c7cp02518a.
2. Edwards, A. J.; Mackenzie, C. F.; Spackman, P. R.; Jayatilaka, D.; Spackman, M. A. Intermolecular interactions in molecular crystals: What's in a name? *Faraday Discuss.* **2017**, *203*, 93–112, doi:10.1039/c7fd00072c.
3. Liu, M.; Li, Q.; Scheiner, S. Comparison of tetrel bonds in neutral and protonated complexes of pyridineTF 3 and furanTF 3 (T = C, Si, and Ge) with NH 3. *Phys. Chem. Chem. Phys.* **2017**, *19*, 5550–5559, doi:10.1039/C6CP07531B.
4. Zierkiewicz, W.; Michalczyk, M.; Scheiner, S. Comparison between tetrel bonded complexes stabilized by σ and π hole interactions. *Molecules* **2018**, *23*, doi:10.3390/molecules23061416.
5. Kolář, M. H.; Hobza, P. Computer Modeling of Halogen Bonds and Other σ-Hole Interactions. *Chem. Rev.* **2016**, acs.chemrev.5b00560, doi:10.1021/acs.chemrev.5b00560.
6. Cavallo, G.; Metrangolo, P.; Milani, R.; Pilati, T.; Priimagi, A.; Resnati, G.; Terraneo, G. The halogen bond. *Chem. Rev.* **2016**, *116*, 2478–2601, doi:10.1021/acs.chemrev.5b00484.
7. Auffinger, P.; Hays, F. a; Westhof, E.; Ho, P. S. Halogen bonds in biological molecules. *Proc. Natl. Acad. Sci. U. S. A.* **2004**, *101*, 16789–16794, doi:10.1073/pnas.0407607101.
8. Politzer, P.; Murray, J. S.; Clark, T. Halogen bonding and other σ-hole interactions: a perspective. *Phys. Chem. Chem. Phys.* **2013**, *15*, 11178–11189, doi:10.1039/c3cp00054k.
9. Guo, X.; Liu, Y. W.; Li, Q. Z.; Li, W. Z.; Cheng, J. B. Competition and cooperativity between tetrel bond and chalcogen bond in complexes involving F2CX (X = Se and Te). *Chem. Phys. Lett.* **2015**, *620*, 7–12, doi:10.1016/j.cplett.2014.12.015.
10. Liu, M.; Li, Q.; Li, W.; Cheng, J.; McDowell, S. A. C. Comparison of hydrogen, halogen, and tetrel bonds in the complexes of HArF with YH3X (X = halogen, y = C and Si). *RSC Adv.* **2016**, *6*, 19136–19143, doi:10.1039/c5ra23556a.
11. Gholipour, A. Mutual interplay between pnicogen–π and tetrel bond in PF3⊥X–Pyr…SiH3CN complexes: NMR, SAPT, AIM, NBO, and MEP analysis. *Struct. Chem.* **2018**, *29*, 1255–1263, doi:10.1007/s11224-018-1106-4.
12. Scheiner, S. Assembly of Effective Halide Receptors from Components. Comparing Hydrogen, Halogen, and Tetrel Bonds. *J. Phys. Chem. A* **2017**, *121*, 3606–3615, doi:10.1021/acs.jpca.7b02305.
13. Tang, Q.; Li, Q. Interplay between tetrel bonding and hydrogen bonding interactions in complexes involving F2XO (X=C and Si) and HCN. *Comput. Theor. Chem.* **2014**, *1050*, 51–57, doi:10.1016/j.comptc.2014.10.025.
14. Del Bene, J. E.; Alkorta, I.; Elguero, J. Exploring the (H2C=PH2)+:N-Base Potential Surfaces: Complexes Stabilized by Pnicogen, Hydrogen, and Tetrel Bonds. *J. Phys. Chem. A* **2015**, *119*, 11701–11710, doi:10.1021/acs.jpca.5b06828.
15. Esrafili, M. D.; Vakili, M.; Javaheri, M.; Sobhi, H. R. Tuning of tetrel bonds interactions by substitution and cooperative effects in XH3Si···NCH···HM (X = H, F, Cl, Br; M = Li, Na, BeH and MgH) complexes. *Mol. Phys.* **2016**, *114*, 1974–1982, doi:10.1080/00268976.2016.1174786.
16. Marín-Luna, M.; Alkorta, I.; Elguero, J. Cooperativity in Tetrel Bonds. *J. Phys. Chem. A* **2016**, *120*, 648–656, doi:10.1021/acs.jpca.5b11876.
17. Solimannejad, M.; Orojloo, M.; Amani, S. Effect of cooperativity in lithium bonding on the strength of

Preprints (www.preprints.org) | NOT PEER-REVIEWED | Posted: 19 October 2018 doi:10.20944/preprints201810.0434.v1

Peer-reviewed version available at *Molecules* **2018**, *24*, 79; doi:10.3390/molecules24010079

halogen bonding and tetrel bonding: (LiCN)n···ClYF3and (LiCN)n···YF3Cl (Y= C, Si and n=1-5) complexes as a working model. *J. Mol. Model.* **2015**, *21*, doi:10.1007/s00894-015-2722-1.

18. Mahmoudi, G.; Bauzá, A.; Frontera, A.; Garczarek, P.; Stilinović, V.; Kirillov, A. M.; Kennedy, A.; Ruiz-Pérez, C. Metal-organic and supramolecular lead(II) networks assembled from isomeric nicotinoylhydrazone blocks: The effects of ligand geometry and counter-ion on topology and supramolecular assembly. *CrystEngComm* **2016**, *18*, 5375–5385, doi:10.1039/c6ce00900j.
19. Wei, Y.; Cheng, J.; Li, W.; Li, Q. Regulation of coin metal substituents and cooperativity on the strength and nature of tetrel bonds. *RSC Adv.* **2017**, *7*, 46321–46328, doi:10.1039/c7ra09881b.
20. Esrafili, M. D.; Mohammadian-Sabet, F. Cooperativity of tetrel bonds tuned by infstituent effects. *Mol. Phys.* **2016**, *114*, 1528–1538, doi:10.1080/00268976.2016.1139207.
21. George, J.; Dronskowski, R. Tetrel bonds in infinite molecular chains by electronic structure theory and their role for crystal stabilization. *J. Phys. Chem. A* **2017**, *121*, 1381–1387, doi:10.1021/acs.jpca.6b12732.
22. Mahmoudi, G.; Dey, L.; Chowdhury, H.; Bauzï¿½, A.; Ghosh, B. K.; Kirillov, A. M.; Seth, S. K.; Gurbanov, A. V.; Frontera, A. Synthesis and crystal structures of three new lead(II) isonicotinoylhydrazone derivatives: Anion controlled nuclearity and dimensionality. *Inorganica Chim. Acta* **2017**, *461*, 192–205, doi:10.1016/j.ica.2017.02.021.
23. Mahmoudi, G.; Gurbanov, A. V.; Rodríguez-Hermida, S.; Carballo, R.; Amini, M.; Bacchi, A.; Mitoraj, M. P.; Sagan, F.; Kukulka, M.; Safin, D. A. Ligand-Driven Coordination Sphere-Induced Engineering of Hybride Materials Constructed from PbCl2 and Bis-Pyridyl Organic Linkers for Single-Component Light-Emitting Phosphors. *Inorg. Chem.* **2017**, *56*, 9698–9709, doi:10.1021/acs.inorgchem.7b01189.
24. Scheiner, S. Systematic Elucidation of Factors That Influence the Strength of Tetrel Bonds. *J. Phys. Chem. A* **2017**, *121*, 5561–5568, doi:10.1021/acs.jpca.7b05300.
25. Dong, W.; Li, Q.; Scheiner, S. Comparative strengths of tetrel, pnicogen, chalcogen, and halogen bonds and contributing factors. *Molecules* **2018**, *23*, 1–17, doi:10.3390/molecules23071681.
26. Scheiner, S. Steric Crowding in Tetrel Bonds. *J. Phys. Chem. A* **2018**, *122*, 2550–2562, doi:10.1021/acs.jpca.7b12357.
27. Southern, S. A.; Bryce, D. L. NMR Investigations of Noncovalent Carbon Tetrel Bonds. Computational Assessment and Initial Experimental Observation. *J. Phys. Chem. A* **2015**, *119*, 11891–11899, doi:10.1021/acs.jpca.5b10848.
28. Caputo, M. C.; Alkorta, I.; Provasi, P. F.; Sauer, S. P. A. Analysis of the interactions in FCCF:(H 2 O) and FCCF:(H 2 O) 2 complexes through the study of their indirect spin–spin coupling constants. *Mol. Phys.* **2018**, *116*, 2396–2405, doi:10.1080/00268976.2018.1488006.
29. Southern, S. A.; Errulat, D.; Frost, J. M.; Gabidullin, B.; Bryce, D. L. Prospects for 207Pb solid-state NMR studies of lead tetrel bonds. *Faraday Discuss.* **2017**, *203*, 165–186, doi:10.1039/C7FD00087A.
30. Scilabra, P.; Kumar, V.; Ursini, M.; Resnati, G. Close contacts involving germanium and tin in crystal structures: experimental evidence of tetrel bonds. *J. Mol. Model.* **2018**, *24*, doi:10.1007/s00894-017-3573-8.
31. Auer, H.; Schlegel, R.; Oeckler, O.; Kohlmann, H. Structural and Electronic Flexibility in Hydrides of Zintl Phases with Tetrel–Hydrogen and Tetrel–Tetrel Bonds. *Angew. Chemie - Int. Ed.* **2017**, *56*, 12344–12347, doi:10.1002/anie.201706523.
32. Laconsay, C. J.; Galbraith, J. M. A valence bond theory treatment of tetrel bonding interactions. *Comput. Theor. Chem.* **2017**, *1116*, 202–206, doi:10.1016/j.comptc.2017.02.017.
33. Chandra, S.; Bhattacharya, A. Attochemistry of Ionized Halogen, Chalcogen, Pnicogen, and Tetrel Noncovalent Bonded Clusters. *J. Phys. Chem. A* **2016**, *120*, 10057–10071, doi:10.1021/acs.jpca.6b09813.

Peer-reviewed version available at *Molecules* **2018**, *24*, 79; doi:10.3390/molecules24010079

34. Kozuch, S.; Nandi, A.; Sucher, A. Ping-Pong Tunneling Reactions: Can Fluoride Jump at Absolute Zero? *Chem. - A Eur. J.* **2018**, doi:10.1002/chem.201802782.
35. Martín-Fernández, C.; Montero-Campillo, M. M.; Alkorta, I.; Elguero, J. Modulating the proton affinity of silanol and siloxane derivatives by tetrel bonds published as part of the journal of physical chemistry virtual special issue "manuel Yáñez and Otilia Mó Festschrift". *J. Phys. Chem. A* **2017**, *121*, 7424–7431, doi:10.1021/acs.jpca.7b07886.
36. Liu, M.; Li, Q.; Li, W.; Cheng, J. Tetrel bonds between PySiX3and some nitrogenated bases: Hybridization, substitution, and cooperativity. *J. Mol. Graph. Model.* **2016**, *65*, 35–42, doi:10.1016/j.jmgm.2016.02.005.
37. Xu, H.-L.; Cheng, J.-B.; Li, H.-B.; Yang, X.; Li, Q.-Z. Tetrel bonds between PhSiF 3 /PhTH 3 (T = Si, Ge, Sn) and H 3 ZO (Z = N, P, As): A pentacoordinate silicon (IV) complex. *Int. J. Quantum Chem.* **2018**, *118*, e25660, doi:10.1002/qua.25660.
38. Grabowski, S. J. Tetrel bonds, penta- and hexa-coordinated tin and lead centres. *Appl. Organomet. Chem.* **2017**, *31*, 1–10, doi:10.1002/aoc.3727.
39. Shen, S.; Zeng, Y.; Li, X.; Meng, L.; Zhang, X. Insight into the π-hole···π-electrons tetrel bonds between F 2 ZO (Z = C, Si, Ge) and unsaturated hydrocarbons. *Int. J. Quantum Chem.* **2018**, *118*, e25521, doi:10.1002/qua.25521.
40. Grabowski, S. J. Tetrel Bonds with π-Electrons Acting as Lewis Bases—Theoretical Results and Experimental Evidences. *Molecules* **2018**, *23*, doi:10.3390/molecules23051183.
41. Del Bene, J. E.; Alkorta, I.; Elguero, J. Carbon-Carbon Bonding between Nitrogen Heterocyclic Carbenes and CO2. *J. Phys. Chem. A* **2017**, *121*, 8136–8146, doi:10.1021/acs.jpca.7b08393.
42. Esrafili, M. D.; Asadollahi, S.; Mousavian, P. Anionic tetrel bonds: An ab initio study. *Chem. Phys. Lett.* **2018**, *691*, 394–400, doi:10.1016/j.cplett.2017.11.051.
43. Scheiner, S. Tetrel Bonding as a Vehicle for Strong and Selective Anion Binding. *Molecules* **2018**, *23*, 1147, doi:10.3390/molecules23051147.
44. Scheiner, S. Comparison of halide receptors based on H, halogen, chalcogen, pnicogen, and tetrel bonds. *Faraday Discuss.* **2017**, *203*, 213–226, doi:10.1039/c7fd00043j.
45. Li, Q.; Guo, X.; Yang, X.; Li, W.; Cheng, J.; Li, H. B. A σ-hole interaction with radical species as electron donors: Does single-electron tetrel bonding exist? *Phys. Chem. Chem. Phys.* **2014**, *16*, 11617–11625, doi:10.1039/c4cp01209g.
46. Del Bene, J. E.; Alkorta, I.; Elguero, J. Anionic complexes of F − and Cl − with substituted methanes: Hydrogen, halogen, and tetrel bonds. *Chem. Phys. Lett.* **2016**, *655–656*, 115–119, doi:10.1016/j.cplett.2016.05.030.
47. Brea, O.; Mó, O.; Yáñez, M.; Alkorta, I.; Elguero, J. Creating σ-Holes through the Formation of Beryllium Bonds. *Chemistry* **2015**, *21*, 12676–82, doi:10.1002/chem.201500981.
48. Marín-Luna, M.; Alkorta, I.; Elguero, J.; Mó, O.; Yáñez, M. Interplay between Beryllium Bonds and Anion-π Interactions in BeR2:C6X6:Y− Complexes (R = H, F and Cl, X = H and F, and Y = Cl and Br). *Molecules* **2015**, *20*, 9961–9976, doi:10.3390/molecules20069961.
49. Del Bene, J. E.; Alkorta, I.; Elguero, J. Halogen bonding involving CO and CS with carbon as the electron donor. *Molecules* **2017**, *22*, doi:10.3390/molecules22111955.
50. Alkorta, I.; Elguero, J.; Del Bene, J. E. Complexes of O=C=S with Nitrogen Bases: Chalcogen Bonds, Tetrel Bonds, and Other Secondary Interactions. *ChemPhysChem* **2018**, *19*, 1886–1894, doi:10.1002/cphc.201800217.

51. Xu, H.; Cheng, J.; Yu, X.; Li, Q. Abnormal Tetrel Bonds between Formamidine and TH3F: Substituent Effects. *ChemistrySelect* **2018**, *3*, 2842–2849, doi:10.1002/slct.201800025.

52. Xu, H.; Cheng, J.; Yang, X.; Liu, Z.; Li, W.; Li, Q. Comparison of σ-Hole and π-Hole Tetrel Bonds Formed by Pyrazine and 1,4-Dicyanobenzene: The Interplay between Anion–π and Tetrel Bonds. *ChemPhysChem* **2017**, *18*, 2442–2450, doi:10.1002/cphc.201700660.

53. Dong, W.; Yang, X.; Cheng, J.; Li, W.; Li, Q. Comparison for σ-hole and π-hole tetrel-bonded complexes involving F2C[dbnd]CFTF3(T[dbnd]C, Si, and Ge): Substitution, hybridization, and solvation effects. *J. Fluor. Chem.* **2018**, *207*, 38–44, doi:10.1016/j.jfluchem.2018.01.003.

54. Wei, Y. X.; Li, H. B.; Cheng, J. B.; Li, W. Z.; Li, Q. Z. Prominent enhancing effects of substituents on the strength of π···σ-hole tetrel bond. *Int. J. Quantum Chem.* **2017**, *117*, doi:10.1002/qua.25448.

55. Esrafili, M. D.; Mohammadian-Sabet, F. Tuning tetrel bonds via cation–π interactions: an ab initio study on concerted interaction in M + –C 6 H 5 XH 3 –NCY complexes (M = Li, Na, K; X = Si, Ge; Y = H, F, OH). *Mol. Phys.* **2016**, *114*, 83–91, doi:10.1080/00268976.2015.1086498.

56. Del Bene, J. E.; Alkorta, I.; Elguero, J. Carbenes as Electron-Pair Donors to CO2for C···C Tetrel Bonds and C-C Covalent Bonds. *J. Phys. Chem. A* **2017**, *121*, 4039–4047, doi:10.1021/acs.jpca.7b03405.

57. Alkorta, I.; Elguero, J.; Del Bene, J. E. Azines as Electron-Pair Donors to CO2for N···C Tetrel Bonds. *J. Phys. Chem. A* **2017**, *121*, 8017–8025, doi:10.1021/acs.jpca.7b08505.

58. Del Bene, J. E.; Elguero, J.; Alkorta, I. Complexes of CO2with the Azoles: Tetrel bonds, Hydrogen bonds and other secondary interactions. *Molecules* **2018**, *23*, 1–14, doi:10.3390/molecules23040906.

59. Servati Gargari, M.; Stilinovic, V.; Bauzá, A.; Frontera, A.; McArdle, P.; Van Derveer, D.; Ng, S. W.; Mahmoudi, G. Design of Lead(II) Metal-Organic Frameworks Based on Covalent and Tetrel Bonding. *Chem. - A Eur. J.* **2015**, *21*, 17951–17958, doi:10.1002/chem.201501916.

60. Grabowski, S. J. Tetrel bond-σ-hole bond as a preliminary stage of the SN2 reaction. *Phys. Chem. Chem. Phys.* **2014**, *16*, 1824–1834, doi:10.1039/c3cp53369g.

61. Szabó, I.; Császár, A. G.; Czakó, G. Dynamics of the F− + CH3Cl → Cl− + CH3F SN2 reaction on a chemically accurate potential energy surface. *Chem. Sci.* **2013**, *4*, 4362, doi:10.1039/c3sc52157e.

62. Stei, M.; Carrascosa, E.; Kainz, M. a.; Kelkar, A. H.; Meyer, J.; Szabó, I.; Czakó, G.; Wester, R. Influence of the leaving group on the dynamics of a gas-phase SN2 reaction. *Nat. Chem.* **2015**, *8*, 1–6, doi:10.1038/nchem.2400.

63. Caballero-García, G.; Romero-Ortega, M.; Barroso-Flores, J. Reactivity of electrophilic chlorine atoms due to sigma-holes: a mechanistic assessment of the chemical reduction of a trichloromethyl group by sulfur nucleophiles. *Phys. Chem. Chem. Phys. Phys. Chem. Chem. Phys* **2016**, *18*, 27300–27307, doi:10.1039/c6cp04321f.

64. Yourdkhani, S.; Jabłoński, M. Revealing the physical nature and the strength of charge-inverted hydrogen bonds by SAPT(DFT), MP2, SCS-MP2, MP2C, and CCSD(T) methods. *J. Comput. Chem.* **2017**, *38*, 773–780, doi:10.1002/jcc.24739.

65. Grabowski, S. J. What Is the Covalency of Hydrogen Bonding? *Chem. Rev.* **2011**, *111*, 2597–2625, doi:10.1021/cr800346f.

66. Zhao, G.-J.; Han, K.-L. Hydrogen bonding in the electronic excited state. *Acc. Chem. Res.* **2012**, *45*, 404–13, doi:10.1021/ar200135h.

67. Mejía, S.; Hernández-Pérez, J. M.; Sandoval-Lira, J.; Sartillo-Piscil, F. Looking inside the intramolecular C-H···O hydrogen bond in lactams derived from α-methylbenzylamine. *Molecules* **2017**, *22*, doi:10.3390/molecules22030361.

Preprints (www.preprints.org) | NOT PEER-REVIEWED | Posted: 19 October 2018 doi:10.20944/preprints201810.0434.v1

Peer-reviewed version available at *Molecules* **2018**, *24*, 79; doi:10.3390/molecules24010079

68. Cruciani, G.; Milletti, F.; Storchi, L.; Sforna, G.; Goracci, L. In silico pKa prediction and ADME profiling. *Chem. Biodivers.* **2009**, *6*, 1812–1821, doi:10.1002/cbdv.200900153.
69. *Computational Drug Discovery and Design*; Baron, R., Ed.; Methods in Molecular Biology; Springer New York: New York, NY, 2012; Vol. 819; ISBN 978-1-61779-464-3.
70. Kim, M. O.; McCammon, J. A. Computation of pH-dependent binding free energies. *Biopolymers* **2016**, *105*, 43–49, doi:10.1002/bip.22702.
71. Ho, J.; Coote, M. L. First-principles prediction of acidities in the gas and solution phase. *Wiley Interdiscip. Rev. Comput. Mol. Sci.* **2011**, *1*, 649–660, doi:10.1002/wcms.43.
72. Alkorta, I.; Legon, A. Nucleophilicities of Lewis Bases B and Electrophilicities of Lewis Acids A Determined from the Dissociation Energies of Complexes B⋯A Involving Hydrogen Bonds, Tetrel Bonds, Pnictogen Bonds, Chalcogen Bonds and Halogen Bonds. *Molecules* **2017**, *22*, 1786, doi:10.3390/molecules22101786.
73. Lange, N. A.; Speight, J. G. *Lange's handbook of chemistry.*; McGraw-Hill, 2005; ISBN 0071432205.
74. Frisch, M. J.; Trucks, G. W.; Schlegel, H. B.; Scuseria, G. E.; Robb, M. A.; Cheeseman, J. R.; Scalmani, G.; Barone, V.; Mennucci, B.; Petersson, G. A.; Nakatsuji, H.; Caricato, M.; Li, X.; Hratchian, H. P.; Izmaylov, A. F.; Bloino, J.; Zheng, G.; Sonnenberg, J. L.; Hada, M.; Ehara, M.; Toyota, K.; Fukuda, R.; Hasegawa, J.; Ishida, M.; Nakajima, T.; Honda, Y.; Kitao, O.; Nakai, H.; Vreven, T.; Montgomery Jr., J. A.; Peralta, J. E.; Ogliaro, F.; Bearpark, M.; Heyd, J. J.; Brothers, E.; Kudin, K. N.; Staroverov, V. N.; Kobayashi, R.; Normand, J.; Raghavachari, K.; Rendell, A.; Burant, J. C.; Iyengar, S. S.; Tomasi, J.; Cossi, M.; Rega, N.; Millam, J. M.; Klene, M.; Knox, J. E.; Cross, J. B.; Bakken, V.; Adamo, C.; Jaramillo, J.; Gomperts, R.; Stratmann, R. E.; Yazyev, O.; Austin, A. J.; Cammi, R.; Pomelli, C.; Ochterski, J. W.; Martin, R. L.; Morokuma, K.; Zakrzewski, V. G.; Voth, G. A.; Salvador, P.; Dannenberg, J. J.; Dapprich, S.; Daniels, A. D.; Farkas, Ö.; Foresman, J. B.; Ortiz, J. V; Cioslowski, J.; Fox, D. J. Gaussian 09, Revision D.01. *Gaussian 09 Rev. D.01, Gaussian Inc.* 2009, Wallingford CT.
75. Lu, T.; Chen, F. Multiwfn: A multifunctional wavefunction analyzer. *J. Comput. Chem.* **2012**, *33*, 580–592, doi:10.1002/jcc.22885.
76. Bader, R. F. W.; Carroll, M. T.; Cheeseman, J. R.; Chang, C. Properties of atoms in molecules: atomic volumes. *J. Am. Chem. Soc.* **1987**, *109*, 7968–7979, doi:10.1021/ja00260a006.